2024 IEEE International Conference on Robotics and Automation (ICRA 2024)
May 13-17, 2024. Yokohama, Japan

Design and Modeling of a Nested Bi-cavity-based Soft Growing Robot for Grasping in Constrained Environments

Haochen Yong, Fukang Xu, Chenfei Li, Han Ding, *Member, IEEE* and Zhigang Wu

Abstract— **Soft growing robots with unique navigation (tip extension by eversion) hold great promise in rescue, medical, and industrial applications. Equipping them with grasping capability would enhance their usefulness in constrained environments for various applications. However, in traditional designs, the tip's eversion naturally conflicts with grasping, and the addition of grippers at the tip would limit navigation inevitably in constrained environments. To realize grasping in such scenes without extra devices, we propose a nested bi-cavity-based growing soft robot (BIBOT). The new design consists of two coaxially nested cavities, where the inner and outer cavities extend synchronously by inversion and eversion of the film rolls. Such a bi-cavity design enables the BIBOT to navigate and grasp without relative movements between the body and environment, and avoids contact between the object and its surroundings as well. Further, a kinematics model is established and verified to precisely control its lengthening and steering by a feed mechanism. Finally, its capability in a constrained environment is demonstrated by navigating and grasping an object in a curved pipe with a variable internal diameter.**

I. Introduction

For many potential applications, e.g., research and rescue [1]–[3], medicine [4]–[6], industry [7], aerospace [8] and nuclear [9], robots are required to be capable of navigating and grasping simultaneously in constrained environments. Continuum robots [10] with flexibility are particularly advantageous in such applications. After decades of development [11], various continuum robots such as tendon-driven robots [12], concentric tube robots [13], rod-driven robots [14], fluid muscle robots [15], and soft growing robots [16] have been proposed. Particularly, pressure-driven soft growing robots [17], the robots growing like vine [18], [19], attracted great attention for navigating in constrained environments due to the following features: (1) extension from the tip remains relatively stationary between the body and the environment [20], (2) extension and recovery along an original path led by the robot's tip in constrained environments [21], and (3) natural softness ensures conformity to the shape of surroundings [22], [23].

From a utilization standpoint, equipping growing robots with grasping capability would be highly beneficial in constrained environments, as it is strongly needed in many scenes, e.g., removing the excised tumors during endoscopic submucosal dissection, entering an aircraft engine to clean up fallen debris, transferring supplies in the rubble, pipeline cleaning, etc. As the robot grows, the tip's eversion pushes objects ahead, conflicting with grasp. The traditional approach is to integrate end-effectors (e.g., camera, light, gripper, forceps) [24], [25] at the tip of the robot. However, unlike other continuum robots, it is hard for soft growing robots to directly fix extra equipment at the moving tip of them via a traditional way (e.g., flange for robotic arm). Jeong et al. [26] designed a novel device that successfully remains attached to a soft growing robot's tip, and realized retrieving and delivering objects. This approach risks damaging the object by contact with its surroundings during retrieval, especially in long, winding paths. Furthermore, the integration of a rigid tip mount will prevent the soft growing robot from squeezing through tight gaps and make it challenging to overcome the extra load [27].

Another feasible approach is to entangle objects without extra equipment, similar to an elephant trunk or an octopus tentacle [28]. A few embodiments can be found in ref [29], [30]. This approach provides some protection for objects, but it requires the robot to be slender enough to entangle the objects in constrained environments. It also loses its advantage in retrieving the object by moving the entire body rather than following the original path led by the robot's tip. For designers, it seems necessary to compromise between the navigation ability and manipulation ability attached to end-effectors. However, as fundamental issues for robots, it is necessary to enable the growing robots to freely navigate and excellently grasp without any compromises in constrained environments.

To approach such a purpose, a novel nested bi-cavity structure is proposed as the core of the so-called nested bi-cavity-based growing soft continuum robot (BIBOT), as shown in Fig. 1. Driven by air pressure, two coaxially nested cavities can extend synchronously under the control of a feed mechanism. Interlayers, the part of the two cavities in contact with each other, will separate at the tip of the BIBOT. For inner and outer cavities, the tip extends through inversion and eversion of interlayers, respectively. Compared to the existing growing robots, such a nested bi-cavity-based design creates a stationary inner cavity environment, and enables wrapping grasping of objects without the integration of extra equipment. The outer cavity would provide natural protection for objects while retrieving. Furthermore, our BIBOT is capable of linear lengthening and controllable steering via a feed mechanism, and is mostly unaffected by air pressure. Therefore, it becomes easier to change the state of the robot by adjusting the inner and outer pressure for better adaptation to the environment. A kinematics model of the lengthening and steering process is established and verified with experiments. Finally, the BIBOT

This research was supported by the National Natural Science Foundation of China under Grant No. 52188102. (*Corresponding author: Zhigang Wu*)

Haochen Yong and Fukang Xu contributed equally to this work.

Haochen Yong, Fukang Xu, Chenfei Li, Han Ding and Zhigang Wu are with the State Key Laboratory of Intelligent Manufacturing Equipment and Technology, Huazhong University of Science and Technology, Wuhan, 430074 China (e-mail: hcyong@hust.edu.cn, m202170500@hust.edu.cn, m202270664@hust.edu.cn, dinghan@hust.edu.cn, zgwu@hust.edu.cn).

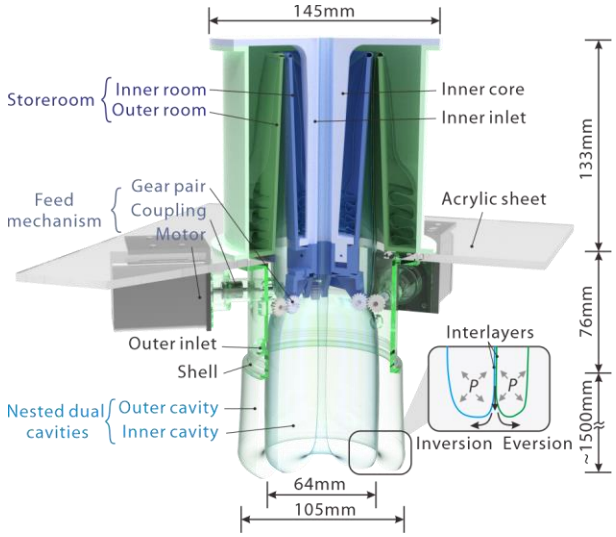

Figure 1. Schematic of the BIBOT. Driven by pressure, two coaxially nested cavities can extend synchronously under the control of the feed mechanism. The subplot shows half of the nested dual cavities, with blue and green lines donating the inner and outer cavities, respectively. For the inner cavity, the tip extends through the inversion of the interlayer, thus enabling wrapping grasping. For the outer cavity, the tip extends through the eversion of the interlayer, thus enabling navigating in constrained environments.

retrieves a target object by navigating in a ~1300 mm long curved pipe with variable internal diameters (95 and 110 mm) to demonstrate the capability of grasping in constrained environments.

The remaining paper is organized as follows: Section II describes the design and principle of the BIBOT and demonstrates the capability of wrapping grasping. Section III presents kinematics analysis and corresponding experimental results, including modeling of lengthening and steering processes. Section IV demonstrates the BIBOT is capable of retrieving an object in constrained environments. Section V concludes the study and provides a discussion of future works.

II. Design and Principle

A. Structure design of BIBOT

As shown in Fig. 1, the BIBOT is mainly composed of three parts: nested dual cavities, a feed mechanism, and a storeroom. The nested dual cavities consist of two coaxially nested cavities. For the inner cavity, one end of the polyethylene (PE) film roll (thickness of 0.05 mm) is stacked and stored in the inner room. The other end passes through the meshing gears and is folded inwards (i.e., inversion), which finally passes through the inner core. Recovering of the inner cavity can be realized by pulling back the part in the inner core. For the outer cavity, one end of the PE film roll of the same thickness is stacked and stored in the outer room, and the other end passes through the meshing gears and is folded outward (i.e., eversion), which finally is fixed to the shell. The maximum external diameter of the inner and outer cavities is 64 and 105 mm, respectively.

The feed mechanism consists of three pairs of meshing gears, each controlled its own motor and evenly distributed around the circumference. The interlayers pass through the meshing gears, fed by the connected motor. To prevent the interlayer from slipping, a silicone rubber sleeve can be wrapped around the gear and thus increase the meshing force of the gears.

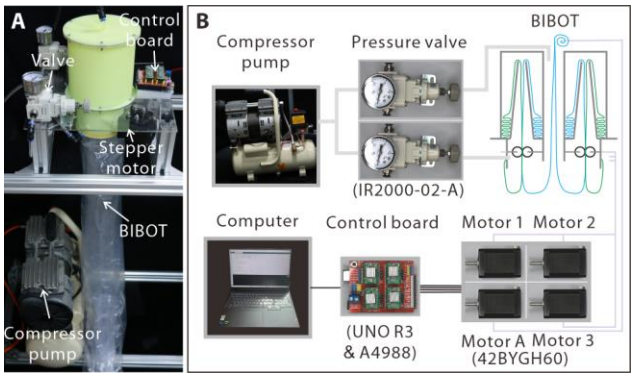

Figure 2. Control block diagram of the BIBOT. (A) In-kind display. (B) Control block diagram. Two pressure valves to regulate the air pressure in the inner and outer cavities. The feed of interlayers is controlled by motor 1~3, and the part of the inner cavity in the inner core is retracted by motor A to recover the inner cavity.

Ref [16] demonstrated a reeled everting vine robot design to keep airtight seal. However, it is difficult to adapt to the dual air cavity structure. Kim et al. [31] proposed a folded storage method that enables robot to implement additional devices, unlike its predecessors, our storeroom consists of two rooms for the storage of PE film rolls. The inverted tilted storeroom design ensures minimized friction between the PE film and the walls of the storeroom under air pressure. The proposed BIBOT can grow up to 1500 mm, depending on the size of the storeroom.

Fig. 2 shows the BIBOT's control block diagram. Compressed gas is generated by a compressor pump and connected to the inner and outer cavities by two parallel independently controlled pressure valves (5 ~ 20 kPa). Three pairs of gears are controlled by the motor 1, 2 and 3. The film in the inner core can be retracted by motor A to realize the recovery of the inner cavity. All stepper motors are controlled by a UNO R3 board with A4988 chips. In this paper, the BIBOT is deployed on a support frame made of aluminum profiles through positioning holes in the acrylic sheet.

B. Growth mechanism based on nested bi-cavity

As shown in Fig. 3 (A), for pressure-driven soft growing robots, we defined two types of growth based on relative relationship between the body and the surroundings: frictional and pave-like growth. A frictional growth (red color) means that the moving side contacts with the wall, while a pave-like growth (green color) means that the still side contacts with the wall, while the moving side paves on the interface. It's obvious that the frictional growth faces greater obstruction than the pave-like growth since the sliding friction between moving sides and the wall increases as the robot grows. Thus, frictional growth should be avoided to reach easier lengthening and a longer navigation distance.

The existing pressure-driven soft growing robots are capable of tip extension by eversion of the material based on single-cavity structure as shown in Fig. 3 (B). Owing to a pave-like growth on the robot-environment surface, it is particularly advantageous in navigation in constrained environments. Unfortunately, the frictional growth on the

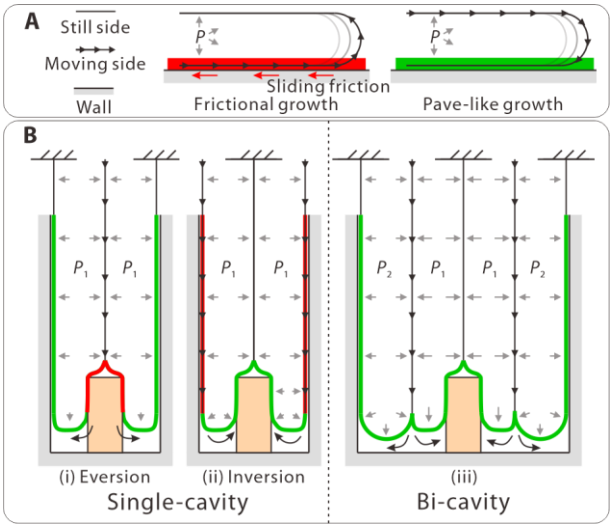

Figure 3. Comparison of the growth based on single-cavity and bi-cavities. (A) Frictional growth (red area) has a relative movement of moving side relative to the wall, and pave-like growth (green area) keeps the still side stationary relative to the wall. (B) Structure of single-cavity and bi-cavity.

robot-object surface naturally conflicts with grasping. One way to realize grasping is to switch eversion into inversion, but inversion makes it hard for the robot to even reach the object as the frictional growth on the robot-environment surface. Therefore, it is difficult for single-cavity-based growing robots to freely navigate and excellently grasp without any compromises.

By combining the above two structures, we proposed a bi-cavity structure consisting two coaxially nested cavities, where the inner and outer cavities extend by the inversion and eversion of materials. This configuration guarantees pave-like growth on both surfaces, allowing excellent grasping as well as free navigation in constrained environments.

C. *Wrapping grasping*

A relatively static inner cavity environment and the inversion of material based on nested bi-cavity realize a wrapping grasping. Fig. 4 (A) shows the typical processes: growing, wrapping, grasping, and recovering. First, the BIBOT approaches objects by growing. Then, upon contact with the object, the inner cavity begins to grow against the object's surface by wrapping. The contact force F on the object can be estimated as

$$F = F_2 - F_1 = P \cdot (\mu S_2 - S_1), \quad (1)$$

where F_1 is the positive pressure on the top of the object from the inner cavity, F_2 is the friction on the side walls of the object, P is the pressure of the inner cavity, μ is the coefficient of static friction between object and PE film, and S_1 and S_2 are the areas of contact at the top and sides, respectively. Afterward, the BIBOT continues to grow until the inner cavity wraps the object completely. F increases as the S_2 increases during the process. Finally, the object is recovered back with the inner cavity, where decreased F_1 leads to a further increase in F, due to the balance of pressure on the top and bottom during the recovery process. Equation (1) hints that lower air pressure facilitates the wrapping of the object, and higher air pressure provides greater force during the grasping process for smooth retrieval of the object.

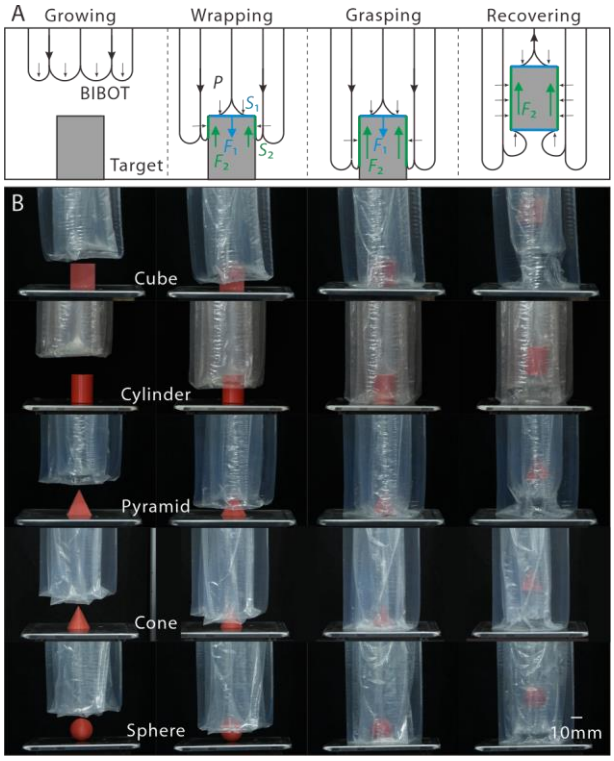

Figure 4. Mechanism and demonstration of wrapping grasping. (A) Force analysis of the wrapping grasping process. (B) Wrapping grasping standard blocks of different shapes in similar size (inner pressure of 5kPa, outer pressure of 2kPa).

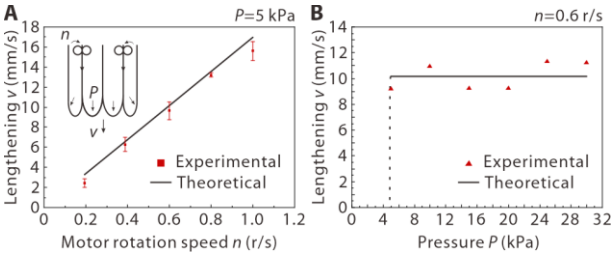

Figure 5. Characterization of the lengthening rate v. (A) The result of lengthening rate v at different motor rotation speed n. (B) The result of lengthening rate v at different pressure P.

Fig. 4 (B) shows the grasping of cubic, cylindrical, pyramid-shaped, conical and spherical standard blocks in similar size (about 30 mm), the weights of the blocks are 14.2 g, 5.9 g, 8.6 g, 4.6g and 7.1 g, respectively. As for the impact of size, we carried out experiments that BIBOT grasp cylindrical standard blocks (height of 38 mm) of different diameters (10 mm, 20 mm, 30 mm and 40 mm), the weights of the cylinders are 1.4 g, 4.2 g, 8.6 g and 15.7 g, respectively. And they are all successfully grasped.

III. KINEMATICS ANALYSIS

A. *Linear lengthening*

In previous works, the relationship between air pressure and growth of soft continuum robots is usually non-linear [16], resulting in technical challenges in control. [32] introduced some methods using stepper motors to make growth speed control robust. Here, we propose a method of growth control: the robot is still pressure-driven growth, but it is precisely

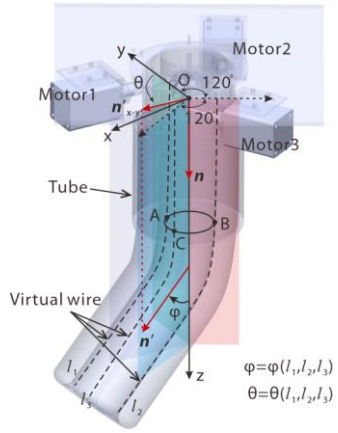

Figure 6. Steering mechanisms of the BIBOT. The length of the three virtual wires is controlled by motors to realize the robot steering in space, and the robot pointing is changed from ***n*** to ***n′***.

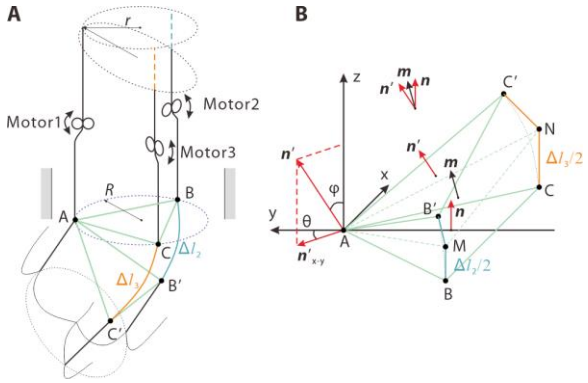

Figure 7. Modeling and analysis of the steering mechanisms. (A) Steering in space due to the length of l_2 and l_3 increase Δl_2 and Δl_3, respectively. The parts above the gears are pulled, causing points from the same cross-section to shift. (B) Geometric relationship between ***n*** and ***n′*** in space.

controlled by the motors. This enables precise control of the growth rate. Considering that the rate of the interlayer is two times the rate of the end of the robot, lengthening rate v of the robot and motor rotation speed n satisfy the following relationship theoretically:

$$v = \frac{1}{2} \cdot n \cdot \pi \cdot d, \tag{2}$$

where d = 10.8 mm is the reference diameter of the gear.

Fig 5. (A) shows that v of the BIBOT is linearly related to n and can be up to ~15.6 mm/s in experiments. Fig 5. (B) shows that the air pressure P does not affect the lengthening rate v. The minimum air pressure value at which the BIBOT can grow is ~5 kPa, and v does not change significantly as P increases. Consequently, we can precisely control the growth rate and decouple the effect of air pressure, which makes it easy to change the state of the robot by adjusting the inner and outer pressure for better adaptation to the environment.

B. Controllable steering

Three pairs of meshing gears independently controlled by motors manage the feeding of the interlayers, and consequently control the active steering of the BIBOT in space. As shown in Fig. 6, three virtual wires are sketched

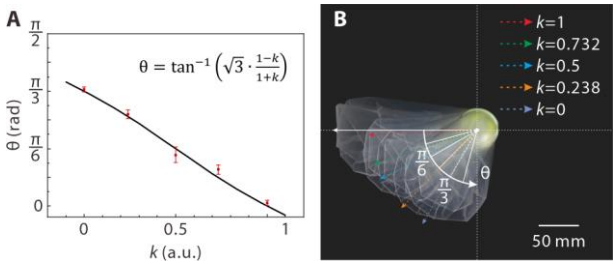

Figure 8. Characterization of plane steering angle θ. (A) The result of plane steering angle θ at different k, where $k=k_3/k_2$. (B) Photographing spatial steering of BIBOT at elevation view, the pressure in both cavities is ~15kPa.

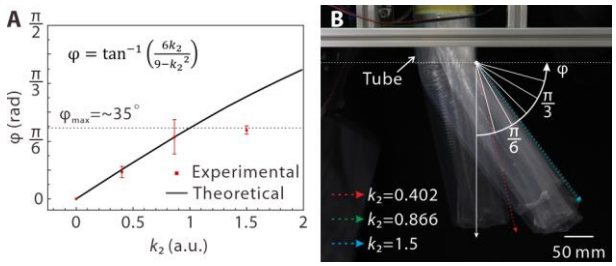

Figure 9. Characterization of spatial rotation angle φ. (A) The result of spatial rotation angle φ at different k_2, where $k_2=k_3$. (B) Photographing spatial steering of BIBOT at front view, the pressure in both cavities is ~15kPa.

along the gear meshing trajectory on the interlayer. The direction of the BIBOT in space is changed from ***n*** to ***n′*** by controlling the length of the three wires (l_1, l_2, and l_3). For the convenience of description, a spatial rectangular coordinate system *O-xyz* is established with *O* as the origin and the direction of ***n*** as the *z*-axis direction. In *O-xyz*, the steering of the BIBOT can be described with the plane steering angle θ and the spatial rotation angle φ, where θ is the angle of $\boldsymbol{n'}_{x\text{-}y}$ (the projection of ***n′*** in the *x-y* plane) and *y*-axis, φ is angle of ***n′*** and *z*-axis. To simplify the kinematics model of the steering process, a few assumptions are made: (1) the inner and outer cavities remain coaxial at all times, ignoring any eccentricity of the inner cavity; (2) the cross-sectional shapes of the inner and outer cavities in the straight segment remain constant; (3) under pressure, the cavities are always under tensile stress and the PE film does not stretch and deform in any directions. The state satisfies or approximately satisfies the above assumptions is defined as a stable state.

Based on the above assumptions, a kinematics model can be described in Fig. 7 (A). Point *A* is fixed, points *B* and *C* grow to the position of points *B'* and *C'*, and the increments of virtual wires passing through points B and C are Δl_2 and Δl_3, respectively. The n and n' are the normal vectors of plane *ABC* and plane *AB'C'*, respectively. As shown in Fig. 7 (B), line segments *CN* and *CN'* are used to approximate arc *CC'*, where *CN* and *NC'* are perpendicular to planes *ABC* and *AB'C'* respectively. Do the same approximation for arc *BB'*. It's easy to get that ***n*** and ***n′*** are symmetrical about ***m*** from the geometric relationship, where m is the normal vector of plane *ANM*. From the second assumption, it can be seen that the equilateral triangle *ABC* is inscribed in the circular section of the interlayer. To simplify the calculation, the origin of the coordinate system *O-xyz* is translated to point *A*. So,

$$\overrightarrow{AM}=\left(-\frac{\sqrt{3}R}{2},-\frac{3R}{2},\frac{\Delta l_2}{2}\right), \tag{3}$$

$$\overrightarrow{AN}=\left(\frac{\sqrt{3}R}{2},-\frac{3R}{2},\frac{\Delta l_3}{2}\right), \tag{4}$$

where R = 32 mm is the radius of inner cavity. Defining dimensionless numbers $k_2 = \Delta l_2/R$, $k_3 = \Delta l_3/R$, we obtain

$$\boldsymbol{m}=\frac{\overrightarrow{AM}\times\overrightarrow{AN}}{\left|\overrightarrow{AM}\times\overrightarrow{AN}\right|}=\left(\frac{\sqrt{3}\left(k_2-k_3\right)}{m},\frac{k_2+k_3}{m},\frac{6}{m}\right), \tag{5}$$

where $m = (3(k_2- k_3)^2+(k_2+ k_3)^2+36)^{1/2}$. From the symmetry relationship, it can be further obtained that

$$\boldsymbol{n'}=2\left|\boldsymbol{m}\cdot\boldsymbol{n}\right|\cdot\boldsymbol{m}-\boldsymbol{n}. \tag{6}$$

Substituting $\boldsymbol{n}$ = (0,0,1) and (5) into (6), we obtain

$$\boldsymbol{n'}=\left(\frac{12\sqrt{3}}{m^2}\left(k_2-k_3\right),\frac{12}{m^2}\left(k_2+k_3\right),\frac{72-m^2}{m^2}\right). \tag{7}$$

From (7) we finally obtain

$$\theta=\tan^{-1}\left(\sqrt{3}\frac{k_2-k_3}{k_2+k_3}\right), \tag{8}$$

$$\varphi=\tan^{-1}\left(\frac{12\sqrt{3\left(k_2-k_3\right)^2+\left(k_2+k_3\right)^2}}{36-3\left(k_2-k_3\right)^2-\left(k_2+k_3\right)^2}\right). \tag{9}$$

Finally, a kinematic model for the BIBOT steering is established.

Due to symmetry, we only need to verify the accuracy of the model within the angles of θ from 0° to 60°. For the rest of the angles, it can be obtained by converting the subscript of the virtual wires in the coordinate system. A new dimensionless number k is defined as $k = k_3/k_2$, so (9) can be rewritten as,

$$\theta=\tan^{-1}\left(\sqrt{3}\frac{1-k}{1+k}\right). \tag{10}$$

Fig. 8 shows that the error between values of θ with different k and the theoretical values is less than 4°. As for φ, we verified the case when $k_3 = k_2$, and (10) can be written as

$$\varphi=\tan^{-1}\left(\frac{6k_2}{9-k_2^{\,2}}\right)\left(k_2=k_3\right). \tag{11}$$

Fig. 9 shows that when φ is less than 30°, the experimental results are very close to the theory. When k increases, the deviation between the experiment and the theory increases. The results indicate that the φ that is consistent with the theoretical value in the stable state is less than ~35°. This phenomenon can be explained as follow. As shown in Fig.7 (A), the interlayer above the gears is distributed on a cylindrical surface with a radius r ($r < R$). When l_2 and l_3 grow, this part will be pulled, and the points originally located on the same section are thus distributed on a slope. To meet the third assumption, this process is unsustainable, therefore, in the stable state, φ cannot continue to increase. The pressure in both cavities is maintained at ~15 kPa. In fact, when the pressure difference between the inner and outer cavities is large enough, the cavities will buckle [21]. In the buckling state, the angle of φ can be greater than 90° by adjusting the inner and outer pressure. This process requires more dedicated dynamic modeling and is not discussed here.

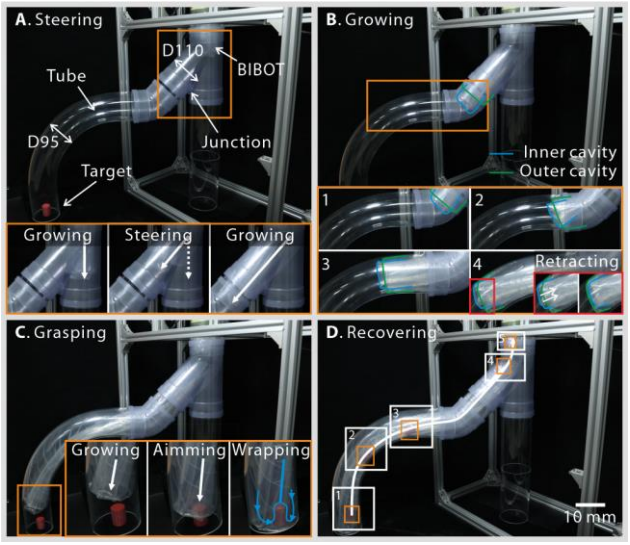

Figure 10. Demonstration of the BIBOT grasping an object in a curved pipe (~1300 mm long) with a variable internal diameter. (A) Active steering at a junction. (B) Passive navigation through a curved pipe, retracting the inner cavity to ensure continued growth. (C) Grasping the target object. (D) Retrieving the object, which is in the protection of the outer cavity, along the original path. The blue and green lines represent the outline of the inner and outer cavities, respectively. A video was attached as well.

IV. Demonstration

A. Experimental settings

To display the ability of the BIBOT to grasp objects in constrained environments, a scenario was set up. As shown in Fig. 10 (A), a reversed Y-shaped pipe with a diameter of 110 mm was fixed beneath the BIBOT. One channel of it is connected to a curved pipe with a diameter of 95 mm and a curvature radius of 420 mm and the other is connected to a straight pipe with the same diameter. A cylinder (height of 38 mm, diameter of 30 mm) was put on the ground as a target in the curved pipe. In this case, the BIBOT must steer at the junction of the Y-shaped pipe based on the model in Section III grow along the curved pipe to reach the target, and then wrap it inside the inner cavity.

B. Wrapping grasping in constrained environments

Fig. 10 shows the demonstration of the BIBOT grasping a cylinder at the end of one curve pipe with open-loop control. First, the BIBOT grew along the straight pipe until reaching the position of the junction (inner pressure of 6 kPa, outer pressure of 5 kPa). At this moment, the air pressure of the outer cavity was released a little to soften it (from 5 kPa to 2 kPa). Motors rotated with different circles to steer the BIBOT. With a softer outer cavity, the BIBOT broke away from one branch of the Y-shaped pipe to another. Then air pressure was restored and BIBOT locked itself in the right path, as shown in Fig. 10 (A).

Afterward, the BIBOT grew steadily, navigating passively along the curved pipe. However, due to the different path

lengths of the inner and outer cavities, the inner cavity will extend beyond the outer cavity. The extended inner cavity would contact the wall of the curved pipe and undergo frictional growth, especially prone to occur on a curved path, which could result in buckling of the inner cavity and stop the growth of the BIBOT. As shown in Fig. 10 (B), when the inner cavity extends longer than the outer cavity, the part of the inner cavity in the inner core should be retracted so that the inner cavity keeps flush with the end of the outer cavity and returns to the protection. This process can be controlled by motor A.

Next, as shown in Fig. 10 (C), the end of the BIBOT reached the target. After aiming, the BIBOT continued growing until the inner cavity wrapped the target entirely. Finally, retracting the part of the inner cavity in the inner core, the target is recovered with the inner cavity while the outer cavity prevents the target from contacting with the pipe, as shown in Fig. 10 (D). A supplementary video is attached.

V. Conclusions and Future Work

Introducing a nested bi-cavity structure, this study proposed a new type of soft growing continuum robot, which is capable of grasping objects smoothly in constrained environments without any compromises in navigation. The feeds of interlayers controlled by the motor enable lengthening rate to be linearly controllable up to ~15.6 mm/s. Further, a kinematic model of the steering process allows precise control of plane steering angle θ in a plane (error < 4°) and achieves a stable spatial rotation angle φ (< ~35°). Finally, in a curved pipe (~1300 mm long) with variable internal diameters, the robot selected the right channel by active steering, and successfully retrieved a 30 mm diameter cylinder by passively navigating. The contributions of this work are as follows.

(1) Designed a nested bi-cavity structure for soft growing robots. It uses the inversion of its inner cavity to create a stationary environment and naturally grasp objects without additional equipment, simultaneously eversion of outer cavity material also retains freely navigation and ensures objects are shielded from surroundings during retrieval.

(2) Established a kinematic model of the new proposed growth and steering processes, achieving precise control of lengthening and steering by a designed feed mechanism, which decouples the effect of air pressure.

(3) Demonstrated the robot capability of freely navigating and excellent grasping in constrained environments just relying on its simple structure with enhanced usefulness.

In the future, dynamics models will be studied further to control robots more precisely. The effect of inner and outer cavity pressure control on robot states and steering ability can be further explored, especially the buckling state that occurs during steering. Further, sensing systems based on vision or flexible sensors can be integrated into the robot system for a closed-loop control.

References

[1] H. Tsukagoshi, A. Kitagawa, and M. Segawa, "Active Hose: an artificial elephant's nose with maneuverability for rescue operation," in *Proceedings 2001 ICRA. IEEE International Conference on Robotics and Automation (Cat. No.01CH37164)*, 2001, pp. 2454–2459 vol.3.

[2] H. Tsukagoshi, N. Arai, I. Kiryu, and A. Kitagawa, "Smooth creeping actuator by tip growth movement aiming for search and rescue operation," *Proc. - IEEE Int. Conf. Robot. Autom.*, pp. 1720–1725, 2011.

[3] N. D. Naclerio, A. Karsai, M. Murray-Cooper, Y. Ozkan-Aydin, E. Aydin, D. I. Goldman, E. W. Hawkes, "Controlling subterranean forces enables a fast, steerable, burrowing soft robot," *Sci. Robot.*, vol. 6, no. 55, p. eabe2922, 2021.

[4] J. Burgner-Kahrs, D. C. Rucker, and H. Choset, "Continuum Robots for Medical Applications: A Survey," *IEEE Trans. Robot.*, vol. 31, no. 6, pp. 1261–1280, 2015.

[5] P. Berthet-Rayne, S. M. H. Sadati, G. Petrou, N. Patel, S. Giannarou, D. R. Leff, C. Bergeles, "Mammobot: A miniature steerable soft growing robot for early breast cancer detection," *IEEE Robot. Autom. Lett.*, vol. 6, no. 3, pp. 5056–5063, 2021.

[6] C. Watson and T. K. Morimoto, "Permanent Magnet-Based Localization for Growing Robots in Medical Applications," *IEEE Robot. Autom. Lett.*, vol. 5, no. 2, pp. 2666–2673, 2020.

[7] L. Li, T. Jin, Y. Tian, F. Yang, and F. Xi, "Design and Analysis of a Square-Shaped Continuum Robot With Better Grasping Ability," *IEEE Access*, vol. 7, pp. 57151–57162, 2019.

[8] M. Wang, X. Dong, W. Ba, A. Mohammad, D. Axinte, and A. Norton, "Design, modelling and validation of a novel extra slender continuum robot for in-situ inspection and repair in aeroengine," *Robot. Comput. Integr. Manuf.*, vol. 67, no. August 2020, p. 102054, 2021.

[9] S. Grazioso, G. Di Gironimo, and B. Siciliano, "Modeling and vibration control of flexible mechanical systems for DEMO remote maintenance: Results from the FlexARM project," *Fusion Eng. Des.*, vol. 146, no. October 2018, pp. 1423–1425, 2019.

[10] G. Robinson and J. B. C. Davies, "Continuum robots - a state of the art," *Proc. - IEEE Int. Conf. Robot. Autom.*, vol. 4, no. May, pp. 2849–2854, 1999.

[11] M. Russo, S. M. H. Sadati, X. Dong, A. Mohammad, I. D. Walker, C. Bergeles, K. Xu, D. A. Axinte, "Continuum Robots: An Overview," *Adv. Intell. Syst.*, vol. 5, no. 5, 2023.

[12] E. Amanov, T. D. Nguyen, and J. Burgner-Kahrs, "Tendon-driven continuum robots with extensible sections—A model-based evaluation of path-following motions," *Int. J. Rob. Res.*, vol. 40, no. 1, pp. 7–23, 2021.

[13] H. Alfalahi, F. Renda, and C. Stefanini, "Concentric Tube Robots for Minimally Invasive Surgery: Current Applications and Future Opportunities," *IEEE Trans. Med. Robot. Bionics*, vol. 2, no. 3, pp. 410–424, 2020.

[14] C. B. Black, J. Till, and D. C. Rucker, "Parallel Continuum Robots: Modeling, Analysis, and Actuation-Based Force Sensing," *IEEE Trans. Robot.*, vol. 34, no. 1, pp. 29–47, 2018.

[15] J. D. Greer, T. K. Morimoto, A. M. Okamura, and E. W. Hawkes, "A Soft, Steerable Continuum Robot That Grows via Tip Extension," *Soft Robot.*, vol. 6, no. 1, pp. 95–108, 2019.

[16] E. W. Hawkes, L. H. Blumenschein, J. D. Greer, and A. M. Okamura, "A soft robot that navigates its environment through growth," *Sci. Robot.*, vol. 2, no. 8, 2017.

[17] E. Del Dottore, A. Sadeghi, A. Mondini, V. Mattoli, and B. Mazzolai, "Toward growing robots: A historical evolution from cellular to plant-inspired robotics," *Front. Robot. AI*, vol. 5, no. MAR, 2018.

[18] D. Weigel and G. Jürgens, "Stem cells that make stems," *Nature*, vol. 415, no. 6873, pp. 751–754, 2002.

[19] M. M. Coad, L. H. Blumenschein, S. Cutler, J. A. R. Zepeda, N. D. Naclerio, H. El-Hussieny, U. Mehmood, J.-H. Ryu, E. W. Hawkes, A. M. Okamura, "Vine Robots," *IEEE Robot. Autom. Mag.*, vol. 27, no. 3, pp. 120–132, 2019.

[20] L. H. Blumenschein, A. M. Okamura, and E. W. Hawkes, "Modeling of Bioinspired Apical Extension in a Soft Robot," in *Biomimetic and Biohybrid Systems*, M. Mangan, M. Cutkosky, A. Mura, P. F. M. J. Verschure, T. Prescott, and N. Lepora, Eds., Cham: Springer International Publishing, 2017, pp. 522–531.

[21] M. M. Coad, R. P. Thomasson, L. H. Blumenschein, N. S. Usevitch, E. W. Hawkes, and A. M. Okamura, "Retraction of Soft Growing Robots Without Buckling," *IEEE Robot. Autom. Lett.*, vol. 5, no. 2, pp. 2115–2122, 2020.

[22] D. A. Haggerty, N. D. Naclerio, and E. W. Hawkes, "Characterizing Environmental Interactions for Soft Growing Robots," *IEEE Int. Conf. Intell. Robot. Syst.*, pp. 3335–3342, 2019.
[23] A. Sadeghi, E. Del Dottore, A. Mondini, and B. Mazzolai, "Passive Morphological Adaptation for Obstacle Avoidance in a Self-Growing Robot Produced by Additive Manufacturing," *Soft Robot.*, vol. 7, no. 1, pp. 85–94, 2020.
[24] S. K. Talas, B. A. Baydere, T. Altinsoy, C. Tutcu, and E. Samur, "Design and Development of a Growing Pneumatic Soft Robot," *Soft Robot.*, vol. 7, no. 4, pp. 521–533, 2020.
[25] D. Mishima, T. Aoki, and S. Hirose, "Development of a pneumatically controlled expandable arm for rescue searches in tight spaces," *Int. J. Rob. Res.*, vol. 25, no. 1, pp. 103–110, 2006.
[26] S. G. Jeong, M. M. Coad, L. H. Blumenschein, M. Luo, U. Mehmood, J. H. Kim, A. M. Okamura, J. H. Ryu, "A tip mount for transporting sensors and tools using soft growing robots," *IEEE Int. Conf. Intell. Robot. Syst.*, pp. 8781–8788, 2020.
[27] W. E. Heap, N. D. Naclerio, M. M. Coad, S. G. Jeong, and E. W. Hawkes, "Soft Retraction Device and Internal Camera Mount for Everting Vine Robots," *IEEE Int. Conf. Intell. Robot. Syst.*, pp. 4982–4988, 2021.
[28] K. Becker, C. Teeple, N. Charles, Y. Jung, D. Baum, J. C. Weaver, L. Mahadevan, R. Wood, "Active entanglement enables stochastic, topological grasping," *Proc. Natl. Acad. Sci. U. S. A.*, vol. 119, no. 42, pp. 1–8, 2022.
[29] S. Kim, Y. Hsiao, Y. Lee, W. Zhu, Z. Ren, F. Niroui, Y. Chen, "Laser-assisted failure recovery for dielectric elastomer actuators in aerial robots," vol. 4278, no. March, 2023.
[30] L. H. Blumenschein, M. Koehler, N. S. Usevitch, E. W. Hawkes, D. C. Rucker, and A. M. Okamura, "Geometric Solutions for General Actuator Routing on Inflated-Beam Soft Growing Robots," *IEEE Trans. Robot.*, vol. 38, no. 3, pp. 1820–1840, 2022.
[31] J. H. Kim, J. Jang, S. M. Lee, S. G. Jeong, Y. J. Kim, and J. H. Ryu, "Origami-inspired New Material Feeding Mechanism for Soft Growing Robots to Keep the Camera Stay at the Tip by Securing its Path," IEEE Robot. Autom. Lett., vol. 6, no. 3, pp. 4592–4599, 2021.
[32] L. H. Blumenschein, M. M. Coad, D. A. Haggerty, A. M. Okamura, and E. W. Hawkes, "Design, Modeling, Control, and Application of Everting Vine Robots," Front. Robot. AI, vol. 7, no. November, pp. 1–24, 2020.